Jong Hwan Lim
Instructor,
Department of
Mechanical Engineering,
Cheju National University,
1 Ara1-dong,
Cheju, 690-756, Korea

Dong Woo Cho
Associate Professor,
Department of
Mechanical Engineering,
Pohang University of
Science and Technology,
San 31 Hyoja-dong, Pohang
790-784, Korea

Specular Reflection Probability in the Certainty Grid Representation

A new method for solving the specular reflection problem of sonar systems has been developed and implemented. This method, the specular reflection probability method, permits the robot to construct a high quality probability map of an environment composed of specular surfaces. The method employs two parameters, the range confidence factor (RCF) and orientation probability. The RCF is the measure of confidence in the returning range from a sensor under reflective environment, and the factor will have low value for long range information and vice versa. Orientation probability represents the surface orientation of an object. Bayesian reasoning is used to update the orientation probability from the range readings of the sensor. The usefulness of this approach is illustrated with the results produced by our mobile robot equipped with ultrasonic sensors.

1 Introduction

Ultrasonic devices have shown utility for object detection in numerous mobile robot researches, as well as in commercial automatic guided vehicles (AGVs). The most popular is the time of the flight (TOF) system, in which the range is computed from the travel time of echo. This system provides an inexpensive means for determining the location of an object. But the range information from a sonar system has much uncertainty due to the wide beam aperture. The first work on this was Moravec's (Moravec and Elfes, 1985). He proposed a probabilistic approach which employed the certainty grid concept and was called an "Ad Hoc" formula. To overcome the incompleteness and to provide a sound theoretical groundwork, a Bayesian updating formula has been developed by Moravec and the author (1988, 1989) and shown to be more efficient and accurate through simulation (Cho, 1990) for construction of a probability map of the robot's surroundings. There was, however, a certain limitation in our earlier model in the real world; the problem of specular reflection, inherent in sonar sensing, was not considered in the sensor model. This effect can be critical for the map quality because most real object surfaces in the real world can be considered as specular (see Section 3).

Moravec and Elfes (1985, 1987) used a simple approach to solve this problem, that is, he discarded range readings above a certain maximum value, assuming the range readings caused by specular reflection are near the maximum ranges. But this method cannot be applied in a wide open area where most of the range readings are maximum ones. On the other hand, Borenstein and Koren (1991) developed another method for reducing the specular reflection effect. Their method is based on the fact that the certainty value of the cell corresponding to the object surface will be high despite many false readings caused by the specular reflection effect if enough range readings are available. The recent work of Kuc and Viard (1991) proposed a maximum obstacle free range within which the specular reflection effect does not occur. Although their methods were successfully applied for fast obstacle avoidance or robot navigation, they could not substantially contribute to improving the map quality due to a great deal of information loss.

In this paper, a new strategy for preventing the specular reflection effect, a modified sensor model for the Bayesian updating formula, is presented which utilizes the specular reflection probability. The specular reflection probability has two components; one is the range confidence factor (RCF), the other is orientation probability. Both of them are related to the confidence in range readings. In the next section we briefly review the Bayesian updating model, and the incompleteness of the earlier model and specular reflection effect are discussed in Section 3. Section 4 introduces the concept of RCF and orientation probability; a complete derivation is given. The derived formulae are verified through a set of experiments in Section 5 and conclusions are drawn in Section 6.

Contributed by the Dynamic Systems and Control Division for publication in the JOURNAL OF DYNAMIC SYSTEMS, MEASUREMENT, AND CONTROL. Manuscript received by the DSCD July 22, 1993. Associate Technical Editor: A. Ray.

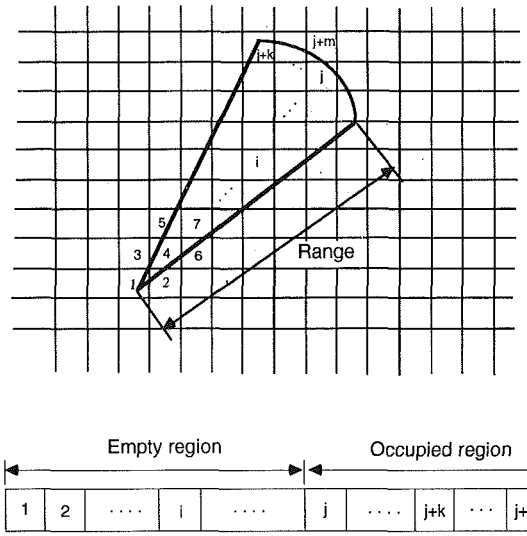

Fig. 1 Rearrangement of the cells according to the distance from the transducer location

2 Review of the Earlier Bayesian Updating Formula

When conditional probability is discussed, we often use the well known Bayes formula (Berger, 1985),

$$P(o|M\cap A) = \frac{P(M|o\cap A)\times P(o|A)}{P(M|o\cap A)\times P(o|A)+P(M|\bar{o}\cap A)\times P(\bar{o}|A)} \quad (1)$$

$$P(\bar{o}|M\cap A) = \frac{P(M|\bar{o}\cap A)\times P(\bar{o}|A)}{P(M|o\cap A)\times P(o|A)+P(M|\bar{o}\cap A)\times P(\bar{o}|A)} \quad (2)$$

where A and M are given conditions and o is another event which is dependent on A and M. In order to apply the above formula to the Bayesian updating model (Moravec and Elfes, 1985, Moravec, 1988), let o be the event that a particular cell in the probability map is occupied by an object, A old information from sensors and M new information about the location of an object. Dividing Eq. (1) by Eq. (2), we have a compact and convenient formulation for computation;

$$\frac{P(o|M\cap A)}{P(\bar{o}|M\cap A)} = \frac{P[M|o\cap A)}{P(M|\bar{o}\cap A)}\times\frac{P(o|A)}{P(\bar{o}|A)} \quad (3)$$

Then Eq. (3) is a formula that inserts new information M into the current probability map consisting of the old information A, i.e., it combines A and M into an estimate of a single quantity $P(o|M\cap A)$. Since $P(\bar{o}|M\cap A)$ in Eq. (3) is the alternative to the probability $P(o|M\cap A)$ and $P(o|A)$, which represents the occupied probability of a cell given old information A, can be retrieved easily from the old map, only $P(o|M\cap A)$ and $P(\bar{o}|M\cap A)$ are left unknown.

Eq. (3) can be rewritten in the form,

$$\frac{P(o_i|M\cap A)}{P(\bar{o}_i|M\cap A)} = \frac{P(M|o_i\cap A)}{P(M|\bar{o}_i\cap A)}\times\frac{P(o_i|A)}{P(\bar{o}_i|A)} \quad (4)$$

where the subscript i represents a certain cell i within the sensor footprint. The cells within the sensor footprint are rearranged according to the distance from the transducer location as in Fig. 1. These cells are divided into two regions: one is an empty region through which the sensor beam must pass, the other is an occupied region where the sensor beam stops. An actual range measurement can possibly be from any cell in the occupied region because of the sensor resolution and the error due to the rasterization of the map into cells. To evaluate $P(M|o_i\cap A)$, the probability that a new measurement M can be obtained assuming that cell i is occupied and A is given, we need to define a new probability $P(H_i|A)$, the probability of the beam halting at cell i, i.e.,

$$P(H_i|A) = P(H_i|o_i)\times P(o_i|A) + P(H_i|\bar{o}_i)\times P(\bar{o}_i|A) \quad (5)$$

where $P(H_i|o_i)$ and $P(H_i|\bar{o}_i)$ are the sensor characteristics. Details of these are given in next section.

Since the beam must pass through the cells in the empty region and stop at a certain cell in the occupied region, we can write $P(M|o_i\cap A)$ as follows (Cho, 1990);

$$P(M|o_i\cap A) = \sum_{n=0}^{m}\prod_{k=1}^{j+n-1} P(\overline{H}_k|o_i\cap A)\,P(H_{j+n}|o_i\cap A)\,P(H_{j+n}|M) \quad (6)$$

where j is the first cell number in occupied region. In a similar way, we obtain,

$$P(M|\bar{o}_i\cap A) = \sum_{n=0}^{m}\prod_{k=1}^{j+n-1} P(\overline{H}_k|\bar{o}_i\cap A)\,P(H_{j+n}|\bar{o}_i\cap A)\,P(H_{j+n}|M) \quad (7)$$

where $P(H_{j+n}|M)$ is the probability that the beam halts at cell $j+n$ in the occupied region. This probability can be assumed to have Gaussian distribution, which implies,

$$\sum_{n=0}^{m} P(H_{j+n}|M) = 1 \quad (8)$$

Now dividing Eq. (6) by Eq. (7), we get the formula:

$$\frac{P(M|o_i\cap A)}{P(M|\bar{o}_i\cap A)} = \frac{\sum_{n=0}^{m}\prod_{k=1}^{j+n-1} P(\overline{H}_k|o_i\cap A)\,P(H_{j+n}|o_i\cap A)\,P(H_{j+n}|M)}{\sum_{n=0}^{m}\prod_{k=1}^{j+n-1} P(\overline{H}_k|\bar{o}_i\cap A)\,P(H_{j+n}|\bar{o}_i\cap A)\,P(H_{j+n}|M)} \quad (9)$$

For a cell in the empty region, Eq. (9) can be reduced to a much simpler one by applying Eq. (5), i.e.,

$$\frac{P(M|o_i\cap A)}{P(M|\bar{o}_i\cap A)} = \frac{P(\overline{H}_i|o_i\cap A)}{P(\overline{H}_i|\bar{o}_i\cap A)} \quad (10)$$

With the aid of the formulae in Eqs. (9) and (10), the probability that a certain cell is occupied can be estimated and updated from Eq. (4) whenever new measurement information is available.

3 Sensor Modeling

In the previous section, we have introduced the probability $P(H_i|A)$, the probability that the beam halts at cell i given the condition of old information A. In this section, every detail for evaluating this probability is given, and the incompleteness of the earlier model is also discussed.

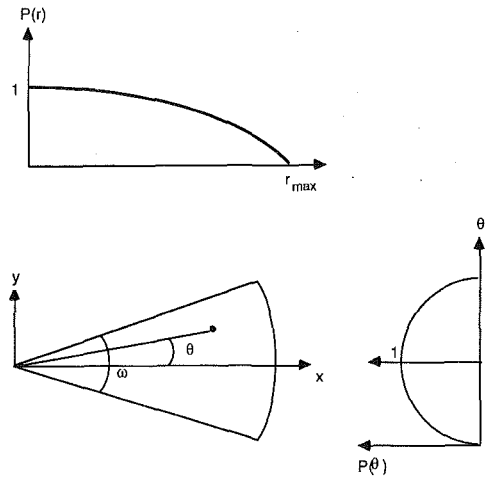

Fig. 2 Probability profiles for P_{DET} and P_{FAL}

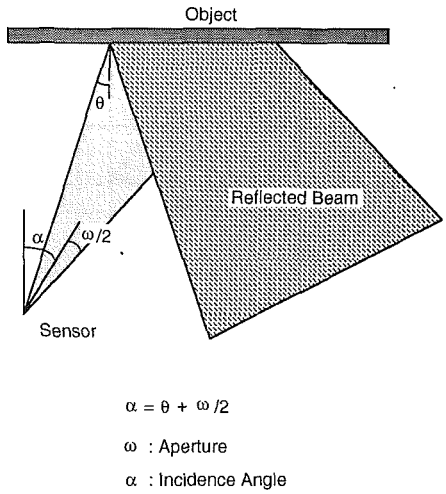

Fig. 3 Anundetected object

3.1 P_{DET} and P_{FAL}. In Eq. (5), $P(H_i|o_i)$ represents the probability of a beam halting at cell i when it is occupied by an object and $P(H_i|\overline{o}_i)$ when it is empty. Denoting $P(H_i|o_i) = P_{DET,i}$ and $P(H_i|\overline{o}_i) = P_{FAL,i}$, Eq. (5) can be rewritten in this form,

$$P(H_i|A) = P_{DET,i}P(o_i|A) = P_{FAL,i}P(\overline{o}_i|A) \qquad (11)$$

Since $P_{DET,i}$ and $P_{FAL,i}$ are characteristics of the sensor, an experimental procedure is needed to accurately determine them. The earlier model, however, adopted an approach modified a little from the Moravec's (1985). That is, $P_{DET,i}$ and $P_{FAL,i}$ values are functions of both the distance from the transducer, and the angle from the transducer axis. Figure 2 shows this relationship:

$$P_{DET} = P(r)\cdot P(\theta) \qquad (12)$$

where

$$P(\theta) = 1 - \left(\frac{\theta}{\omega/2}\right)^2, \text{ for } \theta \in \left[-\frac{\omega}{2}, \frac{\omega}{2}\right]$$

$$P(r) = 1 - \left(\frac{r}{R_{max}}\right)^2, \text{ for } r \in [R_{min}, R_{max}]$$

$P_{FAL} = C \cdot P_{DET}$

ω : effective beam aperture

R_{max} : maximum detection range

R_{min} : minimum detection range

For a commonly used ultrasonic sensor such as Murata (Japan) or Polaroid (frequency of 40 ~ 50 KHz), these assumptions are considered to be reasonable in the sense that the power of the sonar beam has the similar profile to the above.

3.2 Specular Reflection Effect. The ultrasonic sensor returns a radial measure of the distance to the nearest object within the range of detection. The distance is found by measuring the time between transmission of a pulse and the reception of its echo. However, it frequently happens that the sensor fails to detect the nearest object. There are two possible explanations. First, the surface of the object is such that the echo amplitude is too small to be detected by the receiver. Second, the echo pulse is reflected away from the receiver by a surface which is not perpendicular to the transducer axis. This case, which is called "*specular reflection effect*," is more frequent. There are certain object configurations in which an ultrasonic sensor fails to detect the object. As shown in Fig. 3, if we take an object with a specular surface which forms an angle (α) greater than half aperture of the sensor beam ($\omega/2$), the sensor would fail to detect the echo signal (Kuc and Viard, 1991; Walter, 1987; Carlin, 1980). Since the surface of most objects in the real world can be considered as specular according to the following criterion in Eq. (13) in the case of an ultrasonic sensor (Walter, 1987; Nayer et al., 1990) the reflection effect can almost always be observed when the angle of incidence is greater than half the aperture of the beam.

$$\Delta\Omega = \frac{4\pi H}{\lambda}\sin\beta \qquad (13)$$

where,

$\Delta\Omega$: phase difference

λ : wave length

β : $\pi/2$-incidence angle

H : height of surface irregularities

*smooth when $\Delta\Omega < \pi/2$ ($H < 1/8 \sin\beta$)
rough when $\Delta\Omega > \pi/2$ ($H > 1/8 \sin\beta$)

In our earlier model (Moravec and Cho, 1989) of P_{DET} and P_{FAL}, only the attenuation of the power according to the distance and angle is considered. This implies that we put too much confidence in the range information despite the fact that the real world could be highly reflective, so that most of the cells in the resulting map are misleadingly left unoccupied.

4 Modified Sensor Modeling

In this section, a strategy for reducing the specular reflection effect is developed by introducing range confidence and orientation probabilities of objects to modify P_{DET} and P_{FAL} in the real world.

4.1 Confidence for Range Information. Specular reflection effect gives range information that indicates a farther

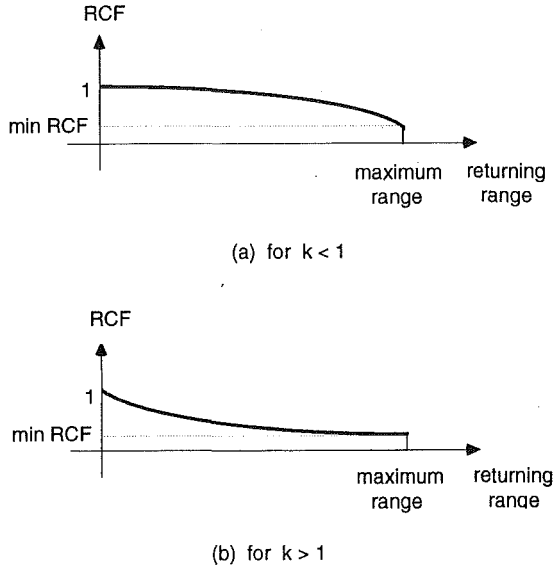

Fig. 4 RCF according to the value of returning range

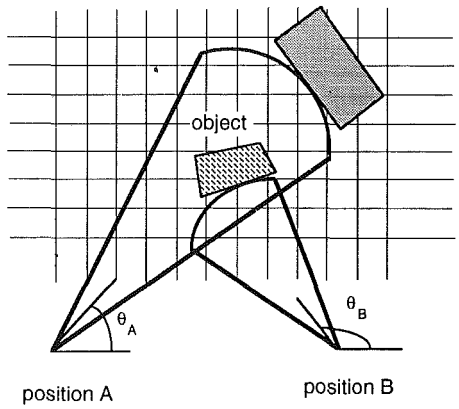

Fig. 5 Extraction of orientation information from returning range

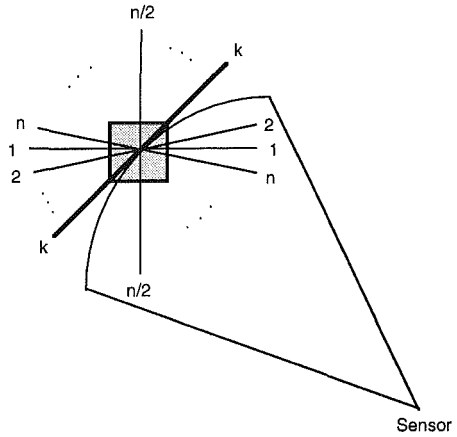

Fig. 6 Schematic diagram of the hypothetical orientations in a cell

location than the actual one. We found that this effect can almost always be observed near the maximum range of the sensor, which led us to interpret long range information as specular reflection occurring with high possibility. In other words, the longer the range, the greater the possibility of the specular reflection effect. For example, in a highly clustered environment, the measured range corresponding to the maximum detection range of the sensor can always be considered as a case of the specular reflection effect.

As shown in Fig. 2, the value of P_{DET} according to r has the same profile regardless of whether the returning range is long or short. However, the confidence in range, in the real world, should be lowered for a longer range value due to the specular reflection effect. This can be performed by introducing Range Confidence Factor (RCF), i.e.,

$$P_{\mathrm{DET,RCF}} = P_{\mathrm{DET}} \times \mathrm{RCF} \tag{14}$$

where, $P_{\mathrm{DET,RCF}}$ is defined as a weighted P_{DET} by the RCF, and

$$\mathrm{RCF} = \left(1 - \frac{\text{returned range}}{\text{max\_detect range} \times \text{range\_weight}}\right)^{k}$$

In the above equation, the range_weight and k, the constants to be determined, are related to the confidence in range information. Figure 4 shows the relationship between the returning range and RCF. The profile of RCF is dependent upon the value of k; for a sensor which not very sensitive RCF would have the similar profile to Fig. 4(a) because once the beam reflects specularly the sensor seldom detects the echo signal, in the contrary, a highly sensitive sensor would have that to Figure 4(b). In the figure, the minimum confidence in range (min RCF) is related to the value of range_weight. For example, if the range_weight is unity, the value of RCF becomes zero when the returning range is maximum. This implies that the maximum range is always caused by specular reflection effect, so that we are not able to utilize that information. But this is not true in a wide open area, where most range readings that are not due to specular reflection will be the maximum one. In this paper, this range_weight, therefore, will be determined through a set of experiments.

4.2 Orientation Probability. As stated in Section 3, the incidence angle of the sensor beam is a major parameter for the specular reflection. Thus the orientation information of a cell, if available, can provide some clue to knowing the incidence angle. We can infer orientation information to some extent from the range information itself, without a priori knowledge about the environment. Figure 5 illustrates that the orientation of an object within an empty region is such that the sensor at position A cannot detect the object while the sensor at position B can. Hence, it is conceivable that the orientation of the object is θ_B and the sensor beam from the other orientation would pass through the object. Likewise, the orientation information can be updated and improved from many range readings by employing the probabilistic approach in the following section.

4.2.1 Orientation Probability. In order to make use of orientation information, we define a new probability $P_v(ori_i^k)$, the probability of cell i being in the kth virtual orientation. The term"virtual" is used to represent our assumption that every cell in the map is occupied and hence has its own orientation. If we divide one cell into n possible orientations as in Fig. 6,, the following holds true for any cell except corners or rounded edges of objects;

$$\sum_{j=1}^{n} P_v(ori_i^j) = 1 \tag{15}$$

Since there are few cells corresponding to edge corners or rounded edges of objects in a map, we can say that Eq. (15) is valid for almost all the cells in the map. Then the actual orientation probability of one cell should be such that,

$$\sum_{j=1}^{n} P(ori_i^j) = P(o_i) \tag{16}$$

because there can be also empty cells that have no orientation, i.e., $\Sigma P(ori) = 0$. The same reasoning as in Section 2 is applied here to evaluate the orientation probability. Let M be a new measurement, k the orientation corresponding to the incidence angle of the beam, thus not causing the specular reflection, and A old information with which to start our reasoning. One form of Bayes' theorem gives,

$$P_v(ori_i^k|M\cap A) = \frac{P_v(M|ori_i^k\cap A)\cdot P_v(ori_i^k|A)}{P_v(M|ori_i^k\cap A)\cdot P_v(ori_i^k|A) + P_v(M|\overline{ori}_i^k\cap A)\cdot P_v(\overline{ori}_i^k|A)} \tag{17}$$

Similarly,

$$P_v(\overline{ori}_i^k|M\cap A) = \frac{P_v(M|\overline{ori}_i^k\cap A)\cdot P_v(\overline{ori}_i^k|A)}{P_v(M|ori_i^k\cap A)\cdot P_v(ori_i^k|M) + P_v(M|\overline{ori}_i^k\cap A)\cdot P_v(\overline{ori}_i^k|A)} \tag{18}$$

Dividing Eq. (17) by Eq. (18), we get the "odds" formula;

$$\frac{P_v(ori_i^k|M\cap A)}{P_v(\overline{ori}_i^k|M\cap A)} = \frac{P_v(M|ori_i^k\cap A)\cdot P_v(ori_i^k|A)}{P_v(M|\overline{ori}_i^k M\cap A)\cdot P_v(\overline{ori}_i^k|A)} \tag{19}$$

In Eq. (19), $P_v(ori_i^k|A)$ is the kth orientation probability of cell i given old information A, which can readily be retrieved from the stored old information.

To evaluate $P_v(M|ori_i^k\cap A)$, the cells in the sensor footprint are rearranged in the same way as in Fig. 1 and accordingly the probability of beam halting at cell i is written as,

$$P_v(H_i|A) = P_v(H_i|ori_i^k)\cdot P_v(ori_i^k|A) + P_v(H_i|\overline{ori}_i^k)\cdot P_v(\overline{ori}_i^k|A) \tag{20}$$

In Eq. (20), $P_v(H_i|ori_i^k)$ is the probability that the beam halts at cell i when $P_v(ori_i^k) = 1$, i.e., the probability that the beam halts at cell i given the conditions that no specular reflection effect is involved and $P(o_i) = 1$. Thus this probability can be replaced with P_{DET} of our earlier model. The same is true between $P_v(H_i|ori_i^k)$ and P_{FAL}. Rewriting Eq. (20), we get,

$$P_v(H_i|A) = P_{\mathrm{DET},i}\cdot P_v(ori_i^k|A) + P_{\mathrm{FAL},i}\cdot P_v(\overline{ori}_i^k|A) \tag{21}$$

With the aid of Eq. (21), $P_v(M|ori_i^k\cap A)$, the probability of a new measurement given $P_v(ori_i^k) = 1$ and old information A, can be found similarly to Eq. (6) in Section 2. That is, the beam must pass through the empty region and stop at one cell in the occupied region. We have,

$$P_v(M|ori_i^k\cap A) = \sum_{n=0}^{m}\prod_{q=1}^{j+n-1} P_v(\overline{H}_q|ori_i^k\cap A)\,P_v(H_{j+n}|ori_i^k\cap A)\,P(H_{j+n}|M) \tag{22}$$

where $P(H_{j+n}|M)$ is the same as for Eq. (8) in Section 2. In a similar way,

$$P_v(M|\overline{ori}_i^k\cap A) = \sum_{n=0}^{m}\prod_{q=1}^{j+n-1} P_v(\overline{H}_q|\overline{ori}_i^k\cap A)\,P_v(H_{j+n}|\overline{ori}_i^k\cap A)\,P(H_{j+n}|M) \tag{23}$$

Dividing Eq. (22) by Eq. (23), we reach the formula;

$$\frac{P_v(M|ori_i^k\cap A)}{P_v(M|\overline{ori}_i^k\cap A)} = \frac{\sum_{n=0}^{m}\prod_{q=1}^{j+n-1} P_v(\overline{H}_q|ori_i^k\cap A)\,P_v(H_{j+n}|ori_i^k\cap A)\,P(H_{j+n}|M)}{\sum_{n=0}^{m}\prod_{q=1}^{j+n-1} P_v(\overline{H}_q|\overline{ori}_i^k\cap A)\,P_v(H_{j+n}|\overline{ori}_i^k\cap A)\,P(H_{j+n}|M)} \tag{24}$$

For a cell in the empty region, inserting Eq. (21) into Eq. (24) and simplifying, we obtain,

$$\frac{P_v(M|ori_i^k\cap A)}{P_v(M|\overline{ori}_i^k\cap A)} = \frac{(1-P_{\mathrm{DET},i})}{(1-P_{\mathrm{FAL},i})} \tag{25}$$

Each one of the last two equations is to be inserted in the "odds" formula in Eq. (19) and thus updates the probability of cell i being in the kth orientation from every new range reading.

4.2.2 Updating Formula for the Other Orientation Probability. The other orientation probabilities, not corresponding to the incidence angle at cell i, should be updated simultaneously for every new range reading. There is a certain relation among the orientation probabilities in one cell as Eq. (15). If $P_v(ori_i^k)$ is updated and increased, the other probabilities should decrease accordingly to satisfy Eq. (15), and vice versa. But the associated increment for each probability should differ according to the angle with orientation k, namely some linear weight is given to each increment; if $P_v(ori_i^k)$ increases, the probability of orientation orthogonal to k should be decreased more than those of others. Correspondingly, the other orientation probabilities are decreased proportionally to the angle with k.

To evaluate the other probabilities, let ΔP be the increment of the probability of the kth orientation. We distribute ΔP to the other orientation probabilities according to their weights, i.e.,

$$P_v(ori_i^m)_{\mathrm{new}} = R\cdot P_v(ori_i^m)_{\mathrm{old}}\cdot\left(1-\Delta P\cdot\frac{w_m}{\sum_{j=1,j\neq k}^{n} w_j}\right) \tag{26}$$

where w_j is the given weight for the jth orientation probability and R is a constant that can be determined by substituting the above equation into Eq. (15), thus giving,

$$\sum_{m=1,\, m\neq k}^{n} P_v(ori_i^m)_{\text{new}} = \sum_{m=1,\, m\neq k}^{n} R \cdot P_v(ori_i^m)_{\text{old}} \cdot \left(1 - \Delta P \cdot \frac{w_m}{\sum_{j=1,\, j\neq k}^{n} w_j} \right) = 1 - P_v(ori_i^k)_{\text{new}} \quad (27)$$

or

$$R = \frac{1 - P_v(ori_i^k)_{\text{new}}}{1 - P_v(ori_i^k)_{\text{old}} - \frac{\Delta P}{\sum_{j=1,\, j\neq k}^{n} w_j} \sum_{j=1,\, j\neq k}^{n} P_v(ori_i^k)_{\text{old}} \cdot w_j} \quad (28)$$

Equation (26) together with Eq. (28) is the updating formula for the orientation probabilities that do not correspond to the incidence angle of the beam at cell i.

4.3 $P_{DET,spec}$ and $P_{FAL,spec}$. Now, considering that the other orientations except kth causes the specular reflection we define $P_{DET,spec,i}$ and $P_{FAL,spec,i}$ as follows: if the kth orientation corresponds to the incidence angle, the specular reflection probability due to orientation is given in the form,

$$P_o(\text{spec}_i) = \sum_{j=1,\, j\neq k}^{n} P_v(ori_i^j) \cdot P(o_i) = \sum_{j=1,\, j\neq k}^{n} P(ori_i^j) \quad (29)$$

Then $P_{DET,ori,i}$ the probability of the beam halting at cell i with $P_o(\text{spec}_i)$ considered, can be defined as follows; $P_{DET,ori,i}$ is dependent on the $P_o(\text{spec}_l)$'s of all the cells before cell i ($l \leq i$), the greatest $P_o(\text{spec}_l)$ among them, however, plays a most dominant role in determining $P_{DET,ori,i}$. In other words, if the specular reflection occurs at a certain cell with a higher $P_o(\text{spec}_l)$ before cell i, $P_o(\text{spec}_i)$ at cell i no longer has a meaning. That is,

$$P_{DET,ori,i} = P_{DET,i} \cdot (1 - \max_{l\leq i} P_o(\text{spec}_l)) \quad (30)$$

Now considering the RCF as well as $P_o(\text{spec}_i)$, $P_{DET,spec,i}$—the specular reflection probability of cell i due to the orientation and RCF—can be defined as,

$$P_{DET,spec,i} = P_{DET,RCF,i}\,(1 - \max_{l\leq i} P_o(\text{spec}_l)) = P_{DET,i}\, P(\overline{\text{spec}_i}) \quad (31)$$

where $P(\text{spec}_i)$ is defined as the *specular reflection probability* of cell i. These last two equations give the modified P_{DET} for a specular environment.

In a similar way in Section 2, $P_{FAL,spec,i}$ is defined as,

$$P_{FAL,spec,i} = CP_{DET,i} \times P(\overline{\text{spec}_i}) = CP_{DET,spec,i} \quad (32)$$

Now we have modified $P(H_i|A)$ by substituting Eqs. (31) to (32) into Eq. (5) in Section 2, i.e.,

$$P(H_i|A) = P_{DET,spec,i} \times P(o_i|A) + P_{FAL,spec,i} \times P(\overline{o}_i|A) \quad (33)$$

Equation (5) in the previous formula can be replaced with Eq. (33) to estimate and update the probability that a certain cell is occupied for a new range information in a reflective environment from the simultaneous use of Eq. (4) and either one of Eqs. (9) and (10).

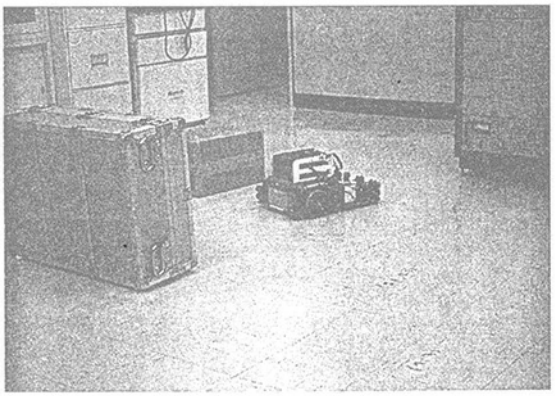

Fig. 7 Picture of GS-boy

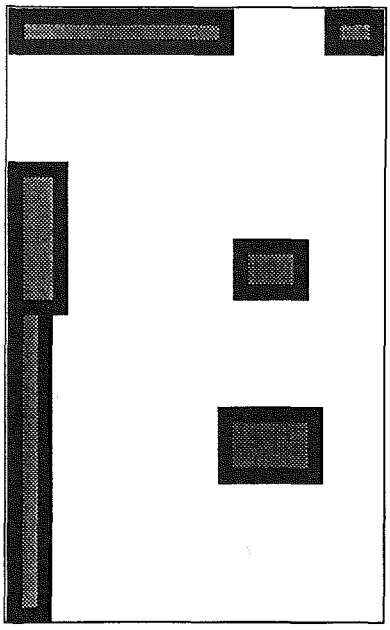

Fig. 8 The true map of experimental environment

5 Experimental Verification

The validity of our reasoning was checked out by implementing and testing the specular reflection probability method on our mobile robot, GS-boy (Gold Star, 1991, Korea), with a dummy wheel at the front and two driving ones at both sides. The position and orientation of the robot are estimated from the each encoder reading of side wheels. The robot is equipped with 9 ultrasonic sensors (Murata, Japan) as in Fig. 7 which have detection ranges of 0.21m to 3.85m. Sensor information from the robot is processed on an IBM-AT compatible 80286 computer. The data sampling interval for each sensor is 0.9 seconds and the robot has a velocity of 0.1 m at its steady state. That is, 9 sets of data are taken every 0.09m. The robot was run following an arbitrary path and 2000 range readings were collected.

Figure 8 shows the true map of the environment which was constructed of a smooth metal box, a paper box, book shelves and walls. The map is composed of 40 × 25 cells

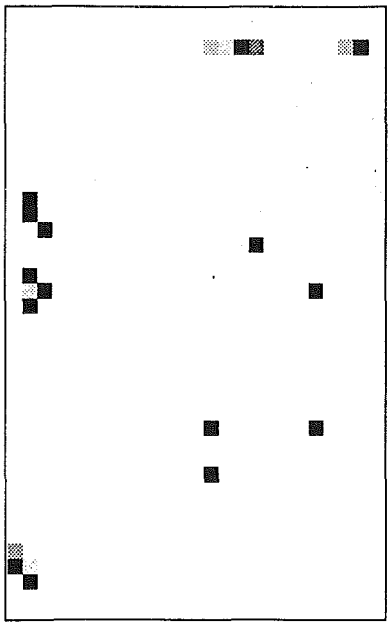

Fig. 9 The reconstructed map from earlier Bayesian model (WM = –4768)

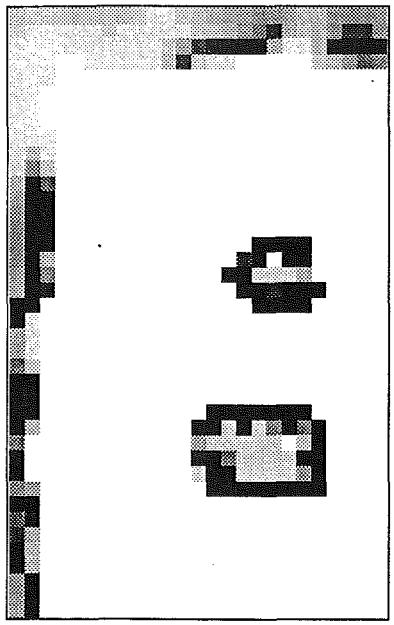

Fig. 10 The reconstructed map by using orientation probability (WM = –840)

and each cell represents a real world square of size 0.18 × 0.18 m^2. The cells are filled with gray levels according to the occupancy probability, that is, blank for empty cells and black for the occupied cells. The inside of each object in the real map is left unknown (P(o) = 0.5) because the sensor can never detect it even in an ideal situation. Figure 9 shows the map reconstructed from the earlier Bayesian model which uses P_{DET} and P_{FAL}. It can be easily seen that most of the objects are undetected due to the specular reflection effect which seriously degrades the map quality.

An indication of the map quality is Weighted Match (WM) between true and reconstructed maps. That is,

$$\text{Weighted Match} = \frac{\text{Match}(e) \times n(o) + \text{Match}(o) \times n(e)}{n(e) + n(o)} \tag{34}$$

where $n(e)$ is the number of empty cells in the true map and $n(o)$ that of occupied cells and Match(.) is defined as (Moravec, 1988),

$$\text{Match}(\cdot) = \log_2 \left(\prod_i \left(P(o_i)_{\text{true}} P(o_i)_{\text{recon}} + P(\overline{o}_i)_{\text{true}} P(\overline{o}_i)_{\text{recon}} \right) \right) \tag{35}$$

Match(o) is evaluated for all occupied cells in the true map and their corresponding cells in the reconstructed map and Match(e) for all empty ones.

The value of WM for the map in Fig. 9 was –4768. On the other hand, when we introduce the orientation probability P_o(spec), WM was –840 as shown in Fig. 10. The use of orientation probabilities drastically enhances the map so that it can be used for robot navigation and simple tasks such as indoor cleaning. One can see, however, that the insides of the objects are not recovered. At the initial stages when most of the cells are unknown, just a little misleading information due to specular reflection can considerably lower the occupancy probabilities of the cells because there is no available orientation information accumulated. The outlines of objects are reconstructed from orientation probability as many readings are stored, but the insides never have a chance to be restored because the beam cannot penetrate the objects' surfaces. In this regard, another factor, RCF, is also considered together with P_o(spec), the specular reflection probability due to cell orientation. Table 1 tabulates the resulting values of WMs for various k and range_weight values when we introduced RCF as well as P_o(spec). From this result 0.8 and 1.1 are determined for k and range_weight, respectively. Figure 11 shows the gradual appearance of an improving map on the screen as the robot moves. One can see that the map quality (WM = –171) is considerably enhanced compared to those of Fig. 9 and Fig. 10. In order to test their validity and applicability these values are applied to an environment composed of more objects than that in Fig. 11. The result is shown in Fig. 12 and the value of WM was –310. For a special environment such as a completely empty space, the above obtained values might not be optimal but they are still able to build a map of the same quality as long as enough range readings are available. Consequently, it can be assumed that k and range_weight are inherent properties of a sensor and independent of the environment if they were determined in a truly randomly arranged environment.

Table 1 WMs for various k and *range_weight* values

k \ range_weight	1.01	1.05	1.1	1.15
0.2	-196	-217	-230	-239
0.4	-174	-183	-192	-198
0.6	-173	-173	-176	-180
0.8	-176	-172	-171	-177
1.0	-178	-174	-172	-175
1.2	-181	-177	-175	-176

6 Conclusion

This paper proposed a new method for reducing specular reflection effects on a sonar sensor. This approach, called

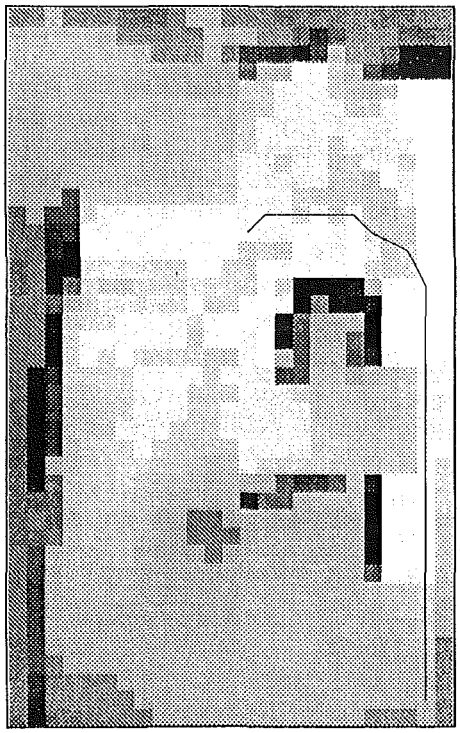

Fig. 11(*a*) Number of readings: 700

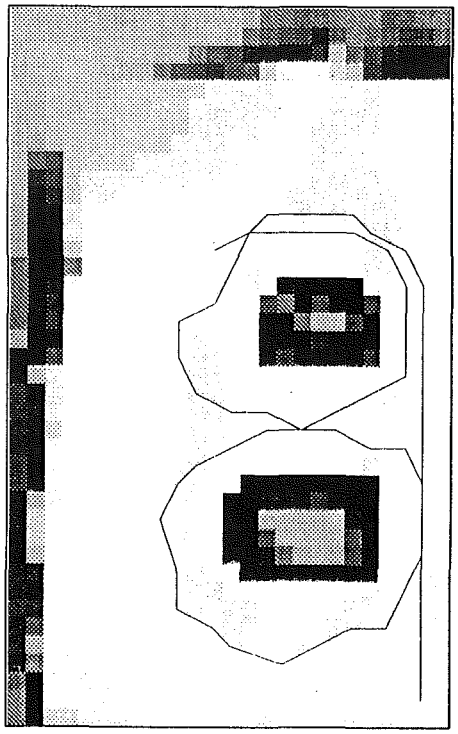

Fig. 11(*c*) Number of readings: 2000(WM = −171)

Fig. 11 The reconstructed maps by using specular reflection probability

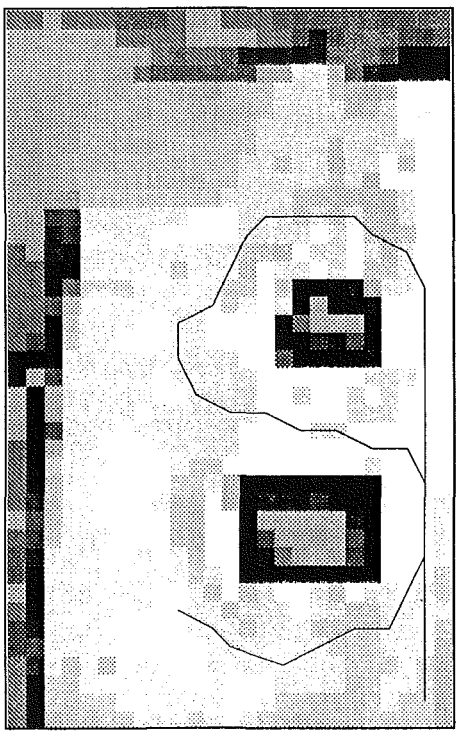

Fig. 11(*b*) Number of readings: 1400

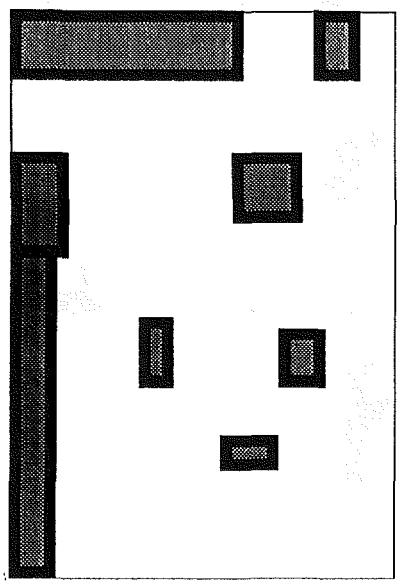

Fig. 12(*a*) The true map

the specular reflection probability method, has been developed and successfully tested through a set of experiments. We introduced a specular reflection probability as a measure of reliability of returning ranges, which enables us to construct the physical sensor model for a real world environment.

The specular reflection probability is based on the following principles;

1) Most of the objects in the real world have highly reflective surfaces, so that the sensor beam would reflect specularly.

2) The range readings caused by specular reflection are often greater than the actual distance of the object. Therefore, the confidence in range reading (RCF) should be such that a longer range reading has lower confidence than a shorter one.

3) The specular reflection effect is mainly due to the relative orientation of an object surface to the transducer

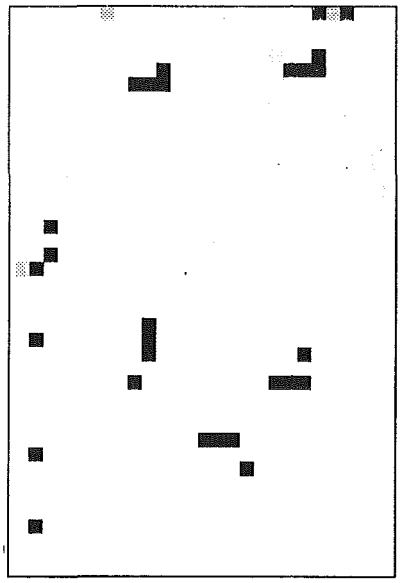

Fig. 12(*b*) The reconstructed map from earlier Bayesian model (WM = −4105)

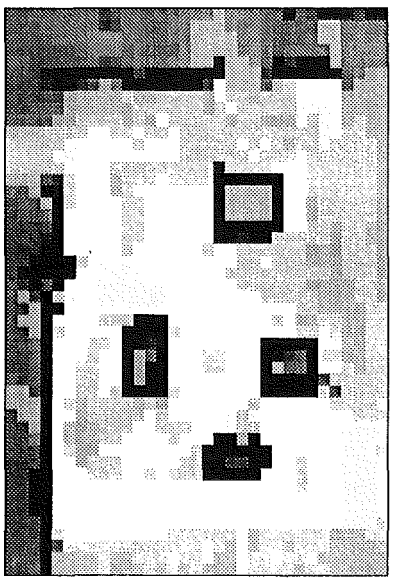

Fig. 12(*c*) The reconstructed map by using specular reflection probability (WM = −420)

Fig. 12 The reconstructed maps of another environment

axis. The range readings from various positions provide information about object orientation, which continuously updates the orientation probability based on Bayesian reasoning.

4) At an initial state of map construction, orientation probability alone gives an incomplete knowledge about specular reflection, because no orientation information is available in that state. Therefore, the RCF plays an important role in such a case.

5) The specular reflection probability will be high in the following cases; i) There exists a cell with high occupation probability in the empty region. ii) The orientation probability perpendicular to the transducer axis is very low. iii) The range reading is long or near the maximum range.

This is an efficient probabilistic method to solve the specular reflection problem and hence enables the robot to construct an accurate map of its surroundings that can be utilized for higher level tasks.

Acknowledgment

This work has been supported by GoldStar Co., Ltd., Korea (1990–1991). We are grateful to Hans P. Moravec of the Carnegie-Mellon University (USA) for providing us with the idea about cell orientations.

References

Berger, J. O., 1985, *Statistical Decision Theory and Bayesian Analysis,* Springer-Verlag, New York.

Borenstein, J., and Koren, Y., 1991, "The Vector Field Histogram—Fast Obstacle Avoidance for Mobile Robots," *IEEE Transaction on Robotics and Automation,* Vol. 7., No. 3, pp. 278–288.

Borenstein, J., and Koren, Y., 1991, "Histogramic In-Motion Mapping for Mobile Robot Obstacle Avoidance," *IEEE Transaction on Robotics and Automation,* Vol. 7, No. 4, pp. 535–539.

Carlin, B., 1980, *Ultrasonics,* McGraw-Hill. New York, NY.

Cho, D. W., 1990, "Certainty Grid Representation for Robot Navigation by a Bayesian Method," *ROBOTICA,* Vol. 8, pp. 159–165.

Elfes, A., "Sonar-Based Real World Mapping and Navigation," *IEEE Transaction on Robotics and Automation,* Vol. RA-3, No. 3, pp. 249–265.

Kuc, R., and Viard, V. B., 1991, "A Physical Based Navigation Strategy for Sonar-Guided Vehicles," *The International Journal of Robotics Research,* Vol. 10, No. 2, pp. 75–87.

Moravec, H. P., 1988, "Sensor Fusion in Certainty Grids for Mobile Robots," *AI Magazine* Vol. 9, No. 2, pp. 61–74.

Moravec, H. P., and Cho, D. W., 1989, "A Bayesian Method for Certainty Grids," *AAAI Spring Symposium on Robot Navigation,* Stanford CA, pp. 57–60.

Moravec, H. P., and Elfes, A., 1985, "High Resolution Maps from Wide Angle Sonar," *IEEE International Conference on Robotics and Automation,* St. Louis, pp. 116–121.

Nayar, S. K., Ikeuchi, K., and Kanade, T., 1990, "Surface Reflection: Physical and Geometrical Perspectives," *Proceedings, Image Understanding Workshop,* Sept. 11–13, pp. 185–212.

Polaroid Corporation, 1982, *Ultrasonic Range Finders,* Polaroid, Cambridge, Mass.

Walter, S. A., 1987, "The Sonar Ring: Obstacle Detection for a Mobile Robot," *IEEE International Conference on Robotics and Automation,* Raleigh NC, pp. 1574–1579.